(Supplementary Material)

Extraction assisted by far infrared radiation and hot air circulation with deep eutectic solvent for bioactive polysaccharides from Poriacocos (Schw.) Wolf

Yingying Guo, [a] Yueshan Li, [b] Zicheng Li, [a] Wentao Yan, [a] Peng Chen, [a] Shun Yao*,[a]

[a] School of Chemical Engineering, Sichuan University, Chengdu, 610065, China

[b] State Key Laboratory of Biotherapy and Cancer Center, West China Hospital, Sichuan University, Chengdu, Sichuan 610041, China.

* Corresponding author, e-mail: Cusack@scu.edu.cn (S. Yao). Tel.: +86-028-85405221; fax: +86-028-85405221

Table of Contents

Conventional auxiliary ways assisted extraction

In the hot solvent extraction of PCP (PCP-DH), the mixture of *poriacocos* powders were evenly mixed and extracted with 50% DES solution for 30 min at 80°C in a DF-101S homothermal system (Yuhua Instrument Co. Ltd, Gongyi, China); in the stirring extraction of PCP (PCP-DS), the same mixture was stirred (1300 rpm) for 30 min at room temperature; ultrasonic assisted extraction (PCP-DU) was carried out in a KQ-400E ultrasonic bath (Kunshan Ultrasonic Instrument Co., Ltd., Suzhou, China) with the power of 400 W for 30 min; microwave assisted extraction (PCP-DM) was carried out on a XH-300UL computerized microwave reactor (Xianghoo Technology Development Co., Ltd, Beijing, China) with the power of 600 W for 30 min. The operation was repeated three times to obtain the average extraction yield of every method.

Electrical conductivity of DESs

Electrical conductivity was determined by a DDS-307A digital conductivity meter (Yueci Electronic Technology Co., Ltd., Shanghai, China). The measurements were carried out for related DESs using a platinized electrode with cell constant of 0.998 cm^{-1} within the range 303~353 K in steps of 10 K in the homothermal system. Moreover, the conductivity meter was calibrated using the standard KCl solution (0.1 mol·L^{-1}). The conductivity of electrolyte was mainly related to the number of conductive ions and the rate of ion migration. Therefore, the conductivity (κ) can be expressed as Eq. (S1).[S1]

$$\kappa = \Sigma n_{\mathrm{i}} m_{\mathrm{i}} q_{\mathrm{i}} \tag{S1}$$

where n_{i}, m_{i} and q_{i} are the number, migration rate and charge number of charged ion i, respectively.

The relationship between the conductivity of every DES and temperature conformed to the Arrhenius equation, which can be expressed as Eq. (S2).[S1]

$$\ln \kappa = \ln \kappa_0 - \frac{E_{\mathrm{A}}}{RT} \tag{S2}$$

where κ_0 is the maximum conductivity at limiting temperature; E_{A} is the activation energy of conductivity; T is the temperature, and R is the gas constant.

Determination of viscosity

For the viscosity-temperature characteristics of solvent are critical properties that directly affect the mass transfer process of target extract,[S2] here the NDJ-8S digital rotary viscometer (Hengping Instrument and Meter Factory, Shanghai, China) was used to perform the rotary viscosity test for three kinds of DESs (ChCl/1,3-But/D-Sor, ChCl/D-Sor and ChCl/1,3-But). The tests were performed at 30~90°C with a temperature interval of 10°C. For this study, the viscosity of DESs was recorded using spindle number 2. The spindle was submerged into the DESs; and then the viscometer measured the resistance (flow viscosity) of the tested DESs at 30 rpm.

Spectral analysis of DESs

FT-IR analysis is widely used to confirm the presence of functional groups or bonds within molecules of the prepared DESs.[S3] These typical groups of new DESs through hydrogen bonding between the chloride ion and hydroxyl compound can be observed in the spectra. In detail, the absorbance bands of 3200~3600 cm^{-1} indicate the presence of O-H stretching in ChCl-based DESs, whereas N-H vibration absorbance overlapped with that of O-H can be found in the range of 3000~3400 cm^{-1}.[S4] The peaks around 1400~1485 cm^{-1} and 1355~1395 cm^{-1} prove the presence of $-CH_2$ and $-CH_3$ bending, respectively. Besides, the saturated ester stretching bonds can be observed in the range of 1100~1300 cm^{-1}.[S3]

As shown in **Fig. S1(c)**, the characteristic peaks of the prepared DESs resemble those of choline chloride, 1,3-butanediol and sorbitol. The details on related FT-IR spectra for all the synthesized DES are listed in **Table S1**. Compared with the three independent components, the broad bands of O-H stretching can be observed after the formation of the DESs, which shift to lower wavenumber for ChCl/D-Sor (3362.69 cm^{-1}), ChCl/1,3-But (3351.37 cm^{-1}) and ChCl/D-Sor/1,3-But (3338.30 cm^{-1}), respectively. This ascribes to the formation of hydrogen bonds in the DESs formation. During the preparation of the DES, the hydroxyl groups (O-H) on 1,3-butanediol or sorbitol interact with chlorine anion (Cl^-) in ChCl hence producing O-H···Cl bonds. Thus, the intensity of the O-H band can be changed by the interaction of H-bond between the quaternary ammonium salt and H-bond donor.[S3] At the same time, as the single donor changes to the composite donor of H-bond, the absorbance of -CH_2 and -CH_3 will shift to higher wavenumber. This can be also affected by the stronger hydrogen bond interaction from composite donor formed within the DES.[S3] As is well known, H-bond is very important for the formation of DES, which can weaken the lattice energy of choline chloride and greatly reduce the melting point of its mixture with polyols, thereby forming a homogeneous liquid under room temperature. The characteristics of DES not only facilitate the mass transfer of natural bioactive components in the medium during the separation process, but also broaden the operational temperature range of the whole process.[S5]

In the ^{1}H NMR spectra (D_2O, 400 MHz), the chemical shift of the hydrogen atoms in every component moves towards the lower field after forming the DES (ChCl/D-Sor/1,3-But, see **Fig. S1(d)**). Among them, the chemical shift (δ_H 3.443) of the hydroxyl group in ChCl changes to δ_H 3.451 (^{1}H NMR of ChCl). In ^{1}H NMR of D-Sor, one of the signals of hydrogen proton of hydroxyl group shifts from δ_H 3.443 to δ_H 3.516. Moreover, the chemical shift (δ 3.454 and δ 3.736) of hydrogen atoms in the hydroxyl group of 1,3-But changes to δ_H 3.678 and δ_H 3.808 (^{1}H NMR of 1,3-But), respectively. In summary, the reason of the signal shift of hydrogen atoms in DES towards lower field is related to the formation of abundant hydrogen bonds, and the findings based on ^{1}H-NMR analysis are consistent with those through FT-IR analysis. Above spectral analysis for the pure DES shows that there is no chemical reaction occurring in its preparation, which accords with previous studies.[S6]

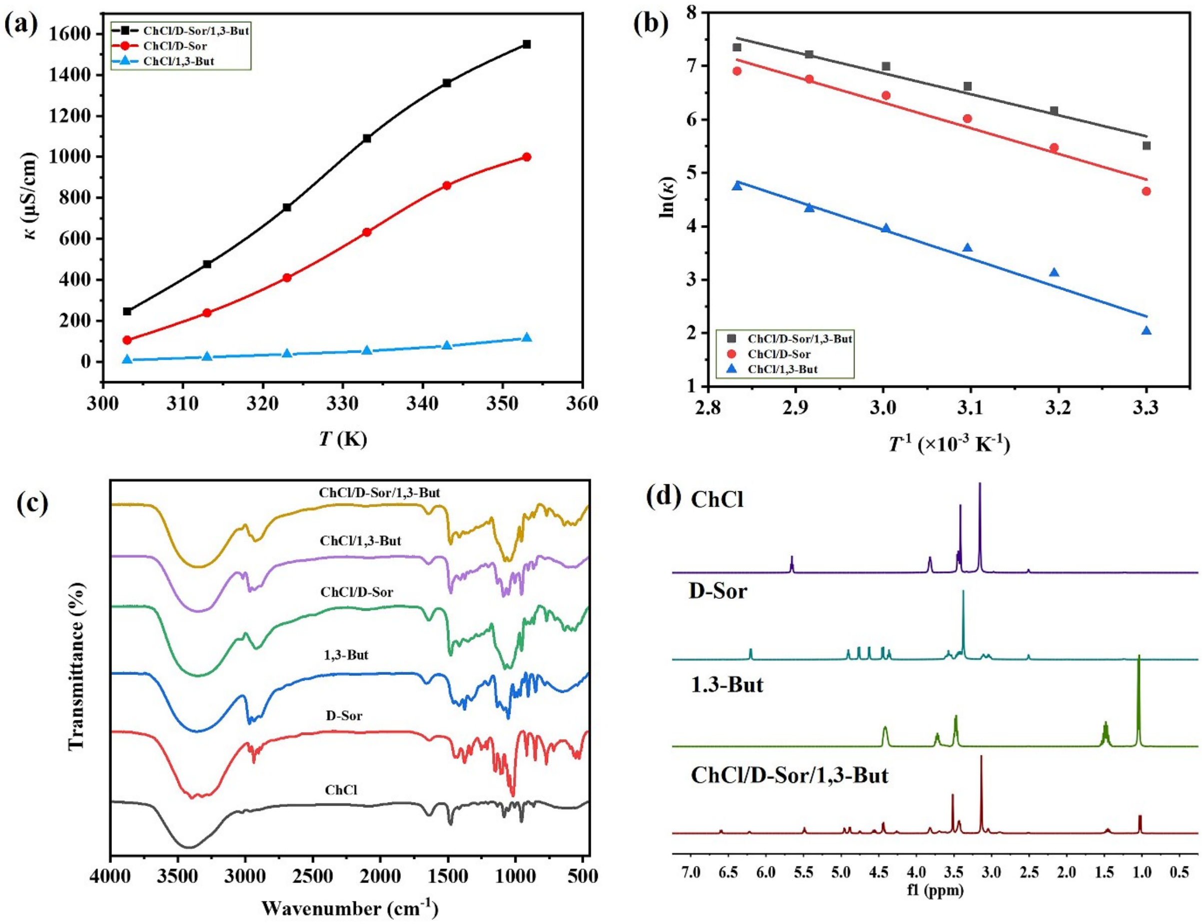

Fig. S1 (a) Influence of temperature on the conductivity of different DESs; (b) relationship of ln*κ* and T^{-1}; (c) FT-IR spectra (KBr disc) of different DESs and their components; (d) ^{1}H NMR of ChCl/D-Sor/1,3-But and its components (D_2O, 400 MHz).

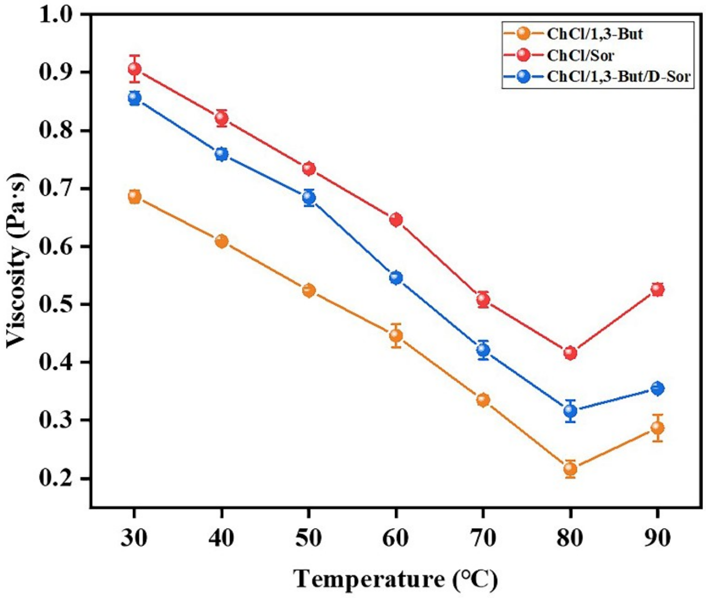

Fig. S2 The viscosity change of three kinds of DESs with the temperature from 30°C to 90°C.

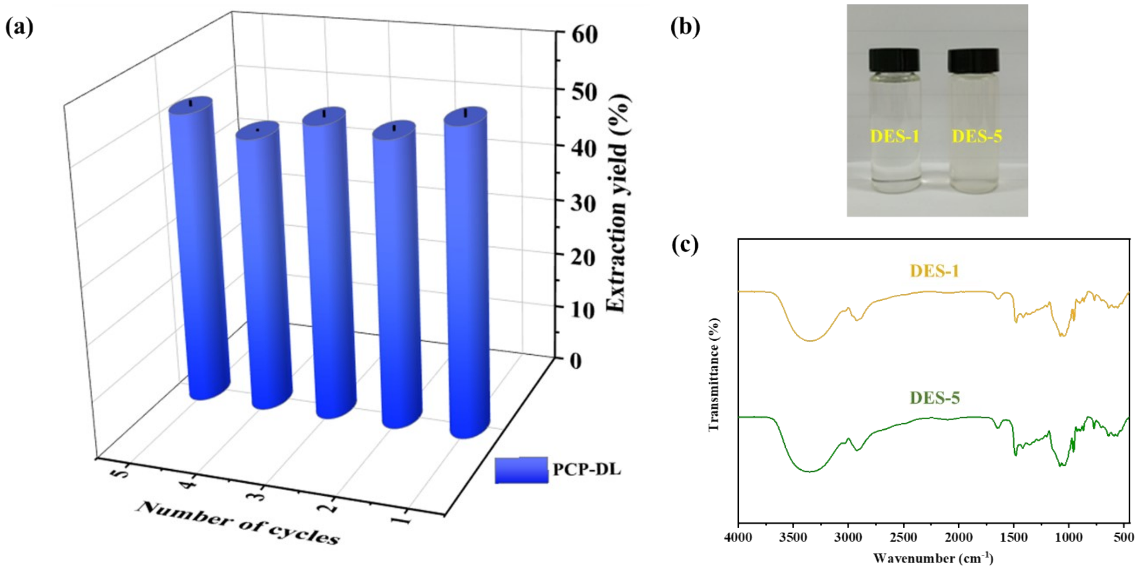

Fig. S3 (a) The change of extraction yield of ChCl/D-Sor/1,3-But in its reuse; the comparison between (b) the status and (c) FT-IR spectra of this extractant recovered for the first (DES-1) and fifth (DES-5) times.

Table S1 Functional groups and wavenumbers of DESs in the FT-IR spectra (KBr disc)

Sample	Wavenumber (cm^{-1})			
	O-H stretching	CH_2 bending	CH_3 bending	C-N stretching
ChCl	3432.5	1470.5	1326.2	1073.6
D-Sor	3389.4	1442.1	-	-
1,3-But	3382.1	1410.5	1327.1	-
ChCl/D-Sor	3362.7	1415.2	1331.4	1071.7
ChCl/1,3-But	3351.4	1471.1	1378.2	1079.1
ChCl/D-Sor/1,3-But	3338.3	1472. 9	1380.4	1078.7

Table S2 Results of orthogonal experimental design (three factors and three levels) for extraction yield

Group	Particle size (mesh)	Liquid-solid ratio (mL/g)	Circulated air temperature (^oC)	Extraction yield (%)
1	400	40	70	48.35
2	200	30	90	44.30
3	400	20	90	47.21
4	200	40	80	50.92
5	300	40	90	46.83
6	400	30	80	53.98
7	300	30	70	47.14
8	300	20	80	51.46
9	200	20	70	44.59

Table S3 The test of inter-subjective effect of three factors

Source	Sum of squares of type III	Df	Mean square	F	Significance (p-value)
Correction model	82.265[a]	6	13.711	91.588	0.011
Intercept	20984.420	1	20984.420	140176.484	0.000
Particle size	16.597	2	8.298	55.433	0.018
Liquid-solid ratio	1.318	2	0.659	4.403	0.185
Circulated air temperature	64.350	2	32.175	214.929	0.005
Error	0.299	2	0.150		
Total	21066.984	9			
Corrected total	82.564	8			

Note: a. R^2=0.996; dependent variable: extraction yield (%).

Table S4 Docking affinity and interaction energy of PCB and three raw materials in DES

Type	Poses[a]	CDOCKER energy	CDOCKER interaction energy	Assessment
1,3-But	1	-0.2713	10.1754	***
	2	-0.3775	**10.2325**	***[b]
	3	-0.3845	10.2181	***
	4	-0.7231	9.0587	**
	5	-1.0881	8.7210	*
	6	-1.3493	10.0850	**
	7	-1.4628	8.5067	*
	8	-1.5279	9.5768	**
	9	-1.5477	8.3532	*
	10	-1.5609	8.2675	*
ChCl	1	7.0090	10.4617	***
	2	6.4896	9.7788	**
	3	5.7120	**11.4473**	****[b]
	4	5.5185	8.8249	**
	5	5.3755	8.6442	*
	6	5.3348	8.5578	*
	7	5.0791	8.2629	*
	8	4.9210	8.1800	*
	9	4.8594	8.1547	*
	10	4.8547	9.3875	**
D-Sor	1	-6.1044	**14.8145**	****[b]
	2	-6.4084	14.1788	****
	3	-7.0990	14.6135	****
	4	-7.3592	13.2818	***
	5	-7.5860	12.9166	***
	6	-7.6409	12.4871	***
	7	-8.7460	11.7521	**
	8	-9.1562	11.9993	**
	9	-9.4341	11.2228	**
	10	-9.8246	10.3199	*

Note: a. 1-10 represent the different docking poses generated by Discovery Studio 3.1 (Accelrys Inc., San Diego, CA, USA); b. optimum pose among all the calculation results.

Table S5 Results of extraction linear regression at different temperatures

Condition	Linear regression equation	R^2	k/min^{-1}
DL-333K	$\ln[C_\infty/(C_\infty-C)]=0.1170x+0.1827$	0.9829	0.1170
DL-343 K	$\ln[C_\infty/(C_\infty-C)]=0.1343x+0.1827$	0.9880	0.1343
DL-353 K	$\ln[C_\infty/(\mathrm{C}_\infty-C)]=0.1744x+0.3458$	0.9946	0.1744
DL-363 K	$\ln[C_\infty/(\mathrm{C}_\infty-C)]=0.1710x+0.2425$	0.9909	0.1710
DL-373 K	$\ln[C_\infty/(C_\infty-C)]=0.1646x+0.0365$	0.9528	0.1646
D-353 K	$\ln[C_\infty/(C_\infty-C)]=0.0787x-0.1388$	0.9787	0.0787
H_2O-353 K	$\ln[C_\infty/(C_\infty-C)]=0.0554x-0.0452$	0.9789	0.0554

Table S6 Inventory for extraction process using Project I and Project II (unit: 100 g PCP product)

Items	Key parameters	Project I	Project II
Operational units	Synthesis of solvents	90°C, 3 h	No pretreatment
	Extraction	Particle size of 300 mesh, liquid (DES)-solid ratio of 30 mL/g, intensity of FIR of 300 W/m^2, and circulated air temperature of 80°C, 0.5 h	Particle size of 300 mesh, liquid (water)-solid ratio of 30 mL/g, 80°C, 0.5 h
	Solid-liquid separation	Suction filtration, 0.1 h	Suction filtration, 0.05 h
	Dialysis	Reset the water every 4 h, 24 h	Reset the water every 4 h, 24 h
	Alcohol precipitation	Add four times the volume of ethanol, -4°C, 12 h	Add four times the volume of ethanol, -4°C, 12 h
	Lyophilization	Vacuum degree of 0.1 Pa at -40°C, 24 h (recovered PCP was 0.43 g/g *poriacocos*)	Vacuum degree of 0.1 Pa at -40°C, 24 h (recovered PCP was 0.041 g/g *poriacocos*)
	Recycling solvents	Concentrate the solution dialysed out of the bag	No pretreatment
Inputs	Raw material (poriacocos powder, kg)	2.50×10^{-1}	2.45
	Choline chloride (kg)	5.98×10^{-1}	0
	1,3-Butanediol (kg)	3.86×10^{-1}	0
	D-sorbitol (kg)	7.80×10^{-1}	0
	Water (kg)	5.20	7.45×10
	Ethanol (kg)	1.26	3.87
	Electricity (kWh)	4.64×10	4.62×10
Outputs	Production of PCP (kg)	1.00×10^{-1}	1.00×10^{-1}
Emissions	Residue (kg)	1.50×10^{-1}	2.35
	Waste water (kg)	5.00	7.31×10
	Waste heat (kJ)	2.05	1.86
	Ethanol (kg)	1.06	3.50

Table S7 Categories impacts used for studies of PCP production using Project I and Project II

Items		Project I	Project II
Shortened form (unit)	Full name		
ADP (kg antimony eq.)	Abiotic depletion potential	×[a]	×
AP (kg SO_2 eq)	Acidification	×	×
CADP (fossil fuel) (kg Coal-R eq.)	Chinese fossil fuel depletion potential	√	√
CADP (kg Coal-R eq.)	Chinese resource depletion potential	×	×
PED (MJ)	Primary energy demand	√[b]	√
CO_2 (kg)	Carbon dioxide	×	×
COD (kg)	Chemical oxygen	×	×
EP (kg PO43-eq)	Eutrophication	×	×
GWP (kg CO_2 eq)	Global warming potential	√	√
IWU (kg)	Industrial water use	×	×
NH_3-N (kg)	Ammomium	×	×
NOx (kg)	Nitrogen oxidation	×	×
RI (kg PM2.5 eq)	Respiratory inorganics	×	×
SO_2 (kg)	Sulfur dioxide	×	×
Waste solids (kg)	Waste solids	√	√
Water use (kg)	Water use	√	√

a. “×” indicates no contribution; b. “√” indicates that the process has influence on this index.

Table S8 Retention time of different dextran standards

Standards	T 40	T 70	T 110	T 500	T 2000	T 3755
Molecular weight (kDa)	40	70	110	500	2000	3755
Retention time (min)	15.00	14.18	14.10	13.02	12.85	12.13

Table S9 HPLC Retention time of standard monosaccharides and those in five products

Monosaccharide	Retention time (min)					
	Standard compound	PCP-DL	PCP-DM	PCP-DU	PCP-DS	PCP-DH
Man	10.169	10.024	10.078	9.895	10.026	10.001
Rha	13.619	-	-	-	-	-
GlcA	16.728	-	-	-	-	-
GalA	20.209	-	-	-	-	-
Glc	24.940	23.772	24.431	23.889	24.303	23.947
Gal	28.976	28.385	28.821	28.080	28.601	28.094
Ara	31.001	-	-	-	-	-

Note: 1. mannose (Man), 2: rhamnose (Rha), 3: glucuronic acid (GlcA), 4: galacturonic acid (GalA), 5: glucose (Glc), 6: galactose (Gal), 7: arabinose (Ara).

Table S10 ^{1}H and ^{13}C NMR chemical shifts of the main residues in PCP-DL (D_2O, 500 MHz)

Residue		Chemical shift, $^{1}H/^{13}C$ δ (ppm)						Reference
		1	2	3	4	5	6	
α-D-Gal*p* (A) (terminal)	H	5.15	3.94	3.80	3.52	3.92	3.94/3.78	S7
	C	102.80	68.60	70.80	70.50	71.40	62.10	
→4)-*α*-D-Gal*p* (B)	H	5.03	3.88	3.71	4.02	4.11	3.94/3.78	S7
	C	99.3	70.2	68.2	78.7	71.0	62.1	
→3)-*β*-D-Glc*p* (C)	H	4.78	3.58	3.77	3.52	3.53	3.74/3.91	S8, S9
	C	102.87	75.46	84.15	68.20	76.44	60.79	
→3,6)-*β*-D-Glc*p* (D)	H	4.76	3.58	3.77	3.59	3.70	3.89/4.22	S8, S9
	C	102.94	73.58	84.15	68.01	75.45	64.43	
→4)-*β*-D-Man*p* (E)	H	4.61	4.04	3.88	3.84	3.64	3.79	S10, S11
	C	103.43	70.54	71.46	76.50	74.15	61.04	

References

S1 P. Nancarrow, A. Al-Othman, D. K. Mital and S. Döpking, *Energy*, 2021, **220**, 119761.

S2 P. Wang, J. Y. Zhang, H. Wen, Z. Y. Zhu, W. Huang and C. K. Liu, *Colloid. Surface. A*, 2021, **610,** 125684.

S3 M. H. Shafie, R. Yusof and C. Y. Gan, *J. Mol. Liq.*, 2019, **288,** 111081.

S4 M. K. Alomar, M. Hayyan, M. A. Alsaadi, S. Akib, A. Hayyan and M. A. Hashim, *J. Mol. Liq.*, 2016, **215,** 98-103.

S5 T. E. Achkar, S. Fourmentin and H. Greige-Gerges, *J. Mol. Liq.*, 2019, **288,** 111028.

S6 D. J. G. P. V. Osch, D. Parmentier, C. H. J. T. Dietz, A. V. D. Bruinhorst, R. Tuinier and M. C. Kroon, *Chem. Commun.*, 2016, **52,** 11987.

S7 T. Y. Lin, M. K. Lu and C. C. Chang, *Int. J. Biol. Macromol.*, 2020, **157,** 311-318.

S8 Y. S. Cui, L. X. Zhu, Y. X. Li, S. L. Jiang, Q. L. Sun, E. Y. Xie, H. B. Chen, Z. Z. Zhao, W. Qiao, J. Xu and C. X. Dong, *Carbohyd. Polym.*, 2021, **255,** 117389.

S9 P. Shao, J. Liu, X. X. Chen, Z. X. Fang and P. L. Sun, *Int. J. Biol. Macromol.*, 2015, **73,** 124-130.

S10 X. T. Fu, H. H. Yang, C. L. Ma, X. Q. Li, D. L. Li, Y. Yang, Y. Q. Xu and L. B. Wang, *Int. J. Biol. Macromol.*, 2020, **163,** 414-422.

S11 L. Feng, J. Y. Yin, S. P. Nie, Y. Q. Wan and M. Y. Xie, *Food Hydrocoll.*, 2018, **76,** 67-77.